Competition Between Intersystem Crossing and Vibrational Cooling in Photoinduced Valence Tautomerism of a Cobalt-Dioxolene Complex Revealed with Femtosecond M-edge XANES

Ryan Ash, Kaili Zhang, Josh Vura-Weis*

Department of Chemistry, University of Illinois at Urbana-Champaign

* Corresponding author: vuraweis@illinois.edu

Abstract

Cobalt complexes that undergo charge-transfer induced spin-transitions (CTIST) or valence tautomerism (VT) from low spin (LS) Co^{III} to high spin (HS) Co^{II} are potential candidates for magneto-optical switches. We use M-edge XANES spectroscopy with 40 fs time resolution to measure the excited-state dynamics of Co^{III}(Cat-N-SQ)(Cat-N-BQ), where Cat-N-BQ and Cat-N-SQ are the singly and doubly reduced forms of the 2-(2-hydroxy-3,5-di-tert-butylphenyl-imino)-4,6-di-tert-butylcyclohexa-3,5-dienone ligand. The extreme ultraviolet probe pulses, produced using a tabletop high-harmonic generation light source, measure 3p→3d transitions and are sensitive to the spin and oxidation state of the Co center. Photoexcitation at 525 nm produces a low-spin Co^{II} ligand-to-metal charge transfer state which undergoes intersystem crossing to high-spin Co^{II} in 67 fs. Vibrational cooling from this hot HS Co^{II} state competes on the hundreds-of-fs timescale with back-intersystem crossing to the ground state, with 60% of the population trapped in a cold HS Co^{II} state for 24 ps. Ligand field multiplet simulations accurately reproduce the ground-state spectra and support the excited-state assignments. This work demonstrates the ability of M-edge XANES to measure ultrafast photophysics of molecular Co complexes.

Introduction

Spin crossover (SCO) in transition metal complexes has gathered considerable attention in the last several decades for its potential use in magneto-optical switching and high-density data storage devices.[1–5] Molecules undergoing SCO exhibit changes in optical and magnetic properties with external stimuli such as temperature, pressure, or light. Upon initiation by a laser pulse, a cascade of coupled electronic and nuclear motion propels a molecular system from a low spin (LS) state into a metastable high spin (HS) state. Most SCO complexes have LS and HS states that only differ in the electron configuration on the metal center, but several cobalt complexes have LS and HS states with a change in the electronic configuration of both the metal and ligands. The difference between the states involves an electron transfer between metal and ligand orbitals, with the phenomenon referred to as a charge-transfer induced spin-transition (CTIST) or valence tautomerism (VT). This class of compounds includes well studied materials such as Co-Fe Prussian Blue analogues and Co dioxolene complexes.[5–9] Dioxolene ligands have valence orbitals close in energy to those of third-row transition metal d orbitals, and can exist in multiple oxidation states. Previous results showed that the electronic structure of the two valence tautomers are localized, and can be thought of as electron transfer between the ligand and metal, with the metal center changing from LS Co^{III} ↔ HS Co^{II}.[10–13]

One such compound that exhibits valence tautomerism is Co^{III}(Cat-N-SQ)(Cat-N-BQ), where Cat-N-BQ is the singly reduced 2-(2-hydroxy-3,5-di-tert-butylphenyl- imino)-4,6-di-tert-butylcyclohexa-3,5-dienone ligand and Cat-N-SQ is the doubly reduced analogue (Figure 1). This molecule interconverts between LS Co^{III}(Cat-N-SQ)(Cat-N-BQ) and HS Co^{II}(Cat-N-$BQ)_2$.[10,14] The LS tautomer is a spin doublet with a radical localized on a single (Cat-N-SQ) ligand, whereas the HS tautomer is a spin quartet with the spin localized on the metal center. For the sake of brevity, both tautomers will be referred to as $Co(DQ)_2$, where DQ is a singly or doubly reduced shiff-base diquinone ligand. Ultrafast optical and infrared transient absorption studies with 200 fs time resolution have shown that upon photoexciting the LS tautomer at 525 nm, the HS state forms in hundreds of femtoseconds.[15,16] An intermediate state was identified in the optical transient absorption (OTA) results with a lifetime of ≤180 fs (potentially limited by the instrument response function), which was suggested to be a LS Co^{II} / oxidized ligand state. However, the multitude of intraligand transitions in the visible region makes assignment of the electronic structure of the Co center difficult. Recent calculations by van Veenendaal of a single Co^{II} atom coupled to a symmetric M-CN vibrational mode suggested that intersystem crossing (ISC) from the Frank-Condon LS Co^{II} state to the metastable HS state could occur within 20 fs, and the Co center might populate higher energy quartet states during relaxation.[17]

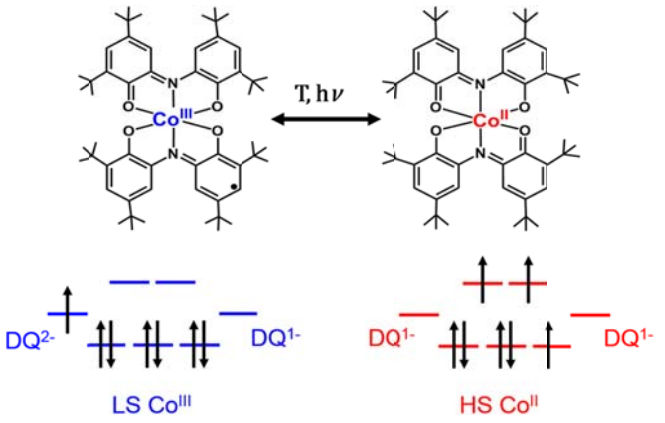

Figure 1: Structure of the two valence tautomers of the $Co(DQ)_2$ system: LS Co^{III}(Cat-N-SQ)(Cat-N-BQ) (left) and HS Co^{II}(Cat-N-$BQ)_2$ (right).

Despite the great interest in Co^{II} systems undergoing CTIST/VT, no transient experiments have been performed that directly probe the electronic state of the metal center with the time resolution necessary to observe the intersystem crossing. Core-level techniques such as L-edge X-ray absorption near-edge structure (XANES) and Kß x-ray fluorescence are sensitive to the spin of the Co center[18,19] and have been successfully used to probe the temperature-dependent spin state of a valence tautomer similar to the one studied here.[11] While femtosecond core-level spectroscopy of Fe complexes has provided important insights into the excited-state electronic structure of molecules such as $Fe(bpy)_3^{2+}$,[20–23] ultrafast experiments at the Co edge are less common.[24–27] The intermediate spin states involved in photoinduced VT have therefore remained elusive.

Extreme ultraviolet (XUV) spectroscopy probes the $M_{2,3}$-edge of third-row transition metals. The 3p → 3d dipole-allowed transitions lying between 30-100 eV contain information about the oxidation state, spin state, and coordination geometry of the metal center, and can be predictably reproduced using ligand-field multiplet (LFM) simulations.[28–31] The development of ultrafast XUV light sources based on high-harmonic generation (HHG) has extended the applicability of $M_{2,3}$-edge spectroscopy to study the dynamics of 3d transition metal complexes. Femtosecond M-edge XANES has been used to measure excited-state relaxation dynamics in Fe and Ni complexes[30,32,33] and in transition metal oxide semiconductors,[34–38] but its applicability to molecular cobalt complexes has not yet been demonstrated. In the present work, we use this emerging technique to measure the mechanism and timescale of ultrafast valence tautomerism in $Co(DQ)_2$ from the perspective of the metal center, revealing an initial LS Co^{II} state that precedes competitive vibrational cooling and intersystem crossing processes.

Methods

$Co(DQ)_2$ was synthesized according to literature procedures,[10] and samples were deposited as ~125 nm thick films on 100 nm Si_3N_4 membranes via vacuum sublimation. The sublimation was performed at $1x10^{-5}$ torr and 210°C, with a deposition rate of 0.1-0.3 Å/s. The complex initially deposits as a mixture of the two valence tautomers, so films were than annealed at 170°C for 30 minutes to convert the majority of the film to the $^1Co^{III}$(Cat-N-SQ)(Cat-N-BQ) phase.

XUV photons for M-edge XANES studies were produced via high-harmonic-generation using the instrument shown in Figure 2A. XUV pulses with a duration of ~15 fs are generated by focusing a Ti:sapphire driving laser pulse (800 nm, 4 mJ, 35 fs, 1 kHz) into a semi-infinite gas cell[39] containing 100 torr Ne. The residual 800 nm photons are attenuated with a Si mirror and 100 nm Al filter. The XUV pulse is then transmitted through the sample and dispersed onto an array CCD. As shown in Figure 2B, the broadband probe spans 40 to 90 eV. Odd harmonics of the 800 nm driving field create peaks every 3.1 eV,[40] but the broad continuum beneath these peaks is suitable for absorption spectroscopy. The spectrometer resolution of roughly 0.3 eV is measured daily by fitting atomic transitions of Xe^+ and Kr^+. The instrument is maintained at a pressure of $<10^{-6}$ torr to prevent absorption of the XUV probe by air. For transient absorption experiments, a fraction of the Ti:sapphire output (0.7 mJ) is fed into a noncollinear optical parametric amplifier (TOPAS White) to generate 10 μJ, 30 fs pulses centered at 525 nm. This pump fluence generates an excitation fraction of ~14%, calculated using the measured absorbance at the pump wavelength. Samples are cooled by a stream of N_2 gas to reduce the effects of accumulative pump laser heating between shots. Time-zero and the instrument

response function (IRF) of 40 fs FWHM were measured by concurrent transient absorption of the IRF-limited LMCT state in α-Fe_2O_3[41].

$M_{2,3}$-edge spectra of transition metal complexes are simulated using ligand field multiplet (LFM) theory.[28,29,31] Briefly, the metal center is modeled using a parametric Hamiltonian containing electron-nuclear and electron-electron coulomb terms, spin-orbit coupling and an electrostatic crystal field. Slater-Condon electron-electron repulsion and mixing parameters were reduced to 60-100% of their free ion values to account for electron delocalization. The simulation assumes an octahedral crystal field with the field splitting parameter 10Dq of 2.7 eV for LS Co^{III} and 1.5 eV for HS Co^{II}. The crystal field splitting for the LS Co^{II} simulation is also set to 2.7 eV to account for its preparation in a Frank-Condon state with the same ligand field as the LS Co^{III} state. Spin-orbit coupling constants were kept the same as the free ion values. Further information about the LFM simulations can be found in the Supporting Information section S2.

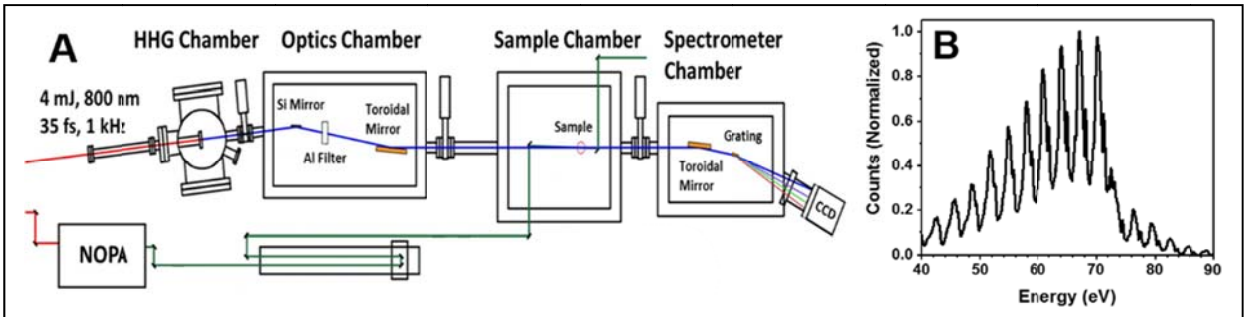

Figure 2: A) Schematic of the XUV spectrometer. XUV photons are produced by high-harmonic generation, then transmitted through a sample and dispersed onto an array CCD. B) Normalized probe spectrum after passing through a 100 nm Si_3N_4 membrane.

Results

Thermal evaporation of $Co(DQ)_2$ produces a film that is a mixture of the low-temperature LS Co^{III} and high-temperature HS Co^{II} tautomers. As shown in Figure 3A, the UV-Vis absorption spectrum of the as-deposited film has peaks at 390, 430 and 530 nm, in addition to a broad absorption feature from 700-800 nm. This low-energy absorption feature is assigned to the HS Co^{II} tautomer[14]. Upon annealing, the 700-800 nm feature disappears and the peaks at 390, 430 and 530 nm rise, indicating conversion from the HS Co^{II} tautomer to the LS Co^{III} tautomer. The annealing process removes the ability of $Co(DQ)_2$ to undergo thermally induced VT, with the film decomposing upon further heating before showing any spectral changes. The film can be redissolved in toluene, showing the same UV-Vis spectra as the synthesized compound and re-exhibiting thermal VT in solution upon heating above room temperature. The bulk solid does not exhibit the same behavior on annealing. The loss of thermal VT on annealing is likely from a change in the molecular packing of the annealed film that increases the energy difference between the two valence tautomers.

Ground state M-edge XANES spectra of the as-deposited and annealed films are shown in Figure 3B. The annealed film has peaks at 65.0, 68.4, and 74.0 eV with a weak shoulder at 61.6 eV. In the as-deposited film, the 74.0 eV peak is attenuated and the 61.6 eV shoulder and main peak gain intensity, with the main peak shifting from 65.0 to 64.4 eV. The difference spectrum ($A_{as\text{-}deposited} - A_{annealed}$) in Figure 3A highlights the changes upon annealing, with a main peak at 62.1 eV, shoulders at 59.9 and 66.4 eV, and a broad negative feature from 70-85 eV. Two independent effects combine to blueshift the LS Co^{III} spectrum relative to HS Co^{II}. First, the increased effective nuclear charge on LS Co^{III} stabilizes the 3p orbitals. As in K-edge and L-edge XANES, an oxidation state change of +1 causes a 1-2 eV blueshift. Second, in the HS Co^{II} state there is increased exchange stabilization of the $3p^5 3d^6$ core-state, which redshifts high-spin spectra relative to their low-spin analogues[28]. These experimental spectral changes are in good agreement with LFM simulations of a combination of HS Co^{II} and LS Co^{III} species. As shown in Figure 3C, the LFM simulation for the HS Co^{II} species ($^4T_{1g}$) predicts a shoulder at 60.0 eV followed by a larger main peak at 63.0 eV. The LS Co^{III} simulation ($^1A_{1g}$) predicts three features of similar intensity at 64.3, 68.7 and 74.3 eV. By forming linear combinations of the simulations and comparing them to the experimental spectra, we estimate the as-deposited film to be a mixture of a 60% HS Co^{II}: 40% LS Co^{III}. When annealed, we estimate this percentage shifts to 10%:90% (Figure 3D). Conveniently, the difference between the experimental annealed and as-deposited spectra gives the expected transient spectrum for photoinduced VT in the $Co(DQ)_2$ system, with shoulders at 59.7 and 65.6 eV, main peak at 62.0 eV and a broad bleach past 68 eV.

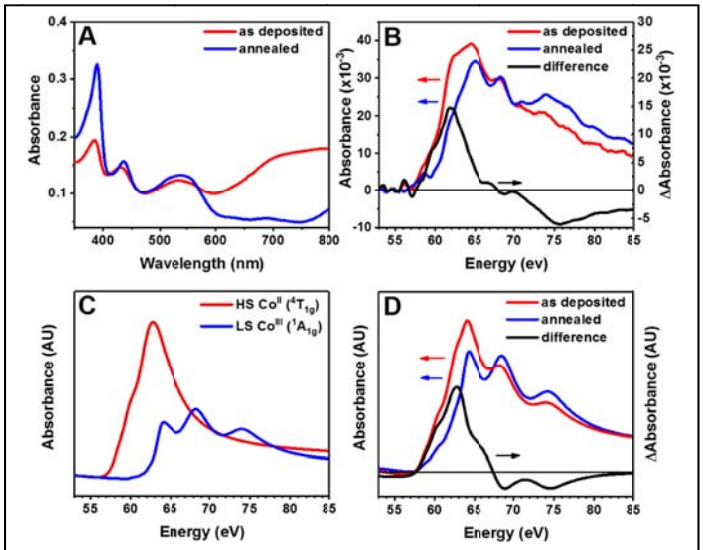

Figure 3: A) UV-Vis spectra of the $Co(DQ)_2$ films as deposited (red) and annealed (blue). B) Ground state M-edge absorption spectrum of the as deposited (red) and annealed (blue) films along with their difference (black). C) LFM simulations for a HS Co^{II} complex (red) and LS Co^{III} complex (blue). D) LFM simulations of the as-deposited (red) and annealed (blue) films by taking a 60%-40% and 10%-90% linear combinations of the HS Co^{II}– LS Co^{III} shown in C. The difference between the simulated spectra is shown in black.

Transient M-edge XANES of $Co(DQ)_2$ after photoexcitation at 525 nm is summarized as a contour plot in Figure 4A, showing the difference in absorption after laser pumping ($A_{pump\ on} - A_{pump\ off}$) as a function of energy and delay time between the pump and probe pulses. As noted in the methods section, absolute t_0 and the instrument response of 40 fs FWHM are measured by fitting the rise of the LMCT state in α-Fe_2O_3. Spectral slices at several delay times are shown in Figure 4B. Initially, a weak induced absorption is observed at 61.5 eV that rises and blueshifts to 62.5 eV within ~100fs. There is also a broad bleach from 73-80 eV that appears at similar timescales. When the blueshift of the positive feature is complete, the transient spectrum is an

excellent match for the difference spectrum between the as-deposited and annealed films, as expected for conversion of LS Co^{III} to HS Co^{II}. Within the first few ps, the transient signal drops by ~40% of the maximum observed value (Figure 5C), then decays further over the next 100 ps, with a weaker, persistent signal with a peak at 63.0 eV lasting longer than the time window of the experiment (> 2 ns).

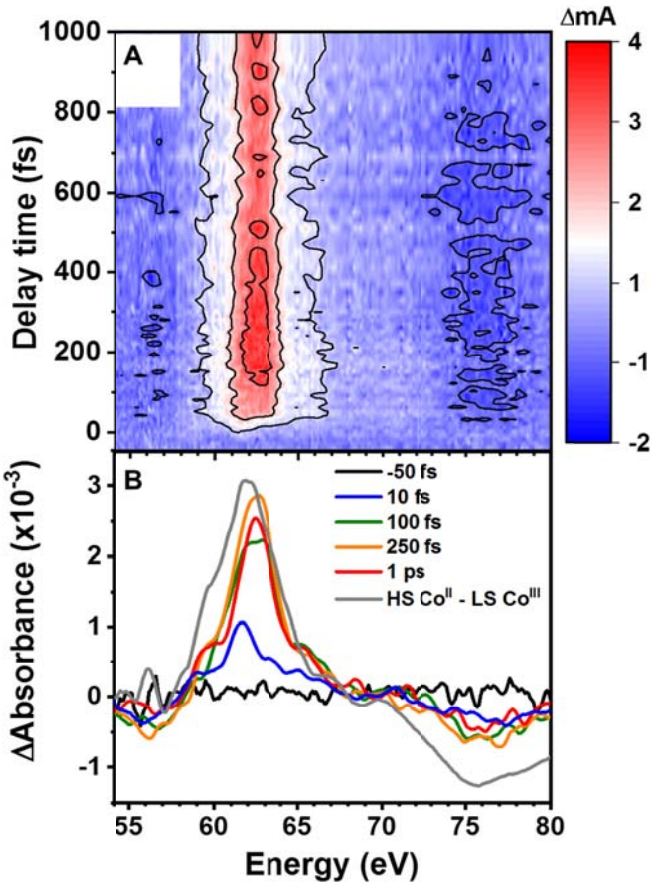

Figure 4: A) Contour plot of transient M-edge XANES of $Co(DQ)_2$. B) Spectral slices within the first picosecond of laser excitation, showing a delayed rise of a feature that shifts to higher energies then reduces in intensity after a few hundred femtoseconds. The transient spectrum at 250 fs and beyond is similar in shape to the difference spectrum between annealed and unannealed films shown in gray.

The data was first fit to a 4-state $A \overset{k_1}{\rightarrow} B \overset{k_2}{\rightarrow} C \overset{k_3}{\rightarrow} D$ sequential model in which the final component accounts for the persistent long-time transient signal. Time zero and the 40 fs instrument response function are fixed to the values obtained from concurrent transient absorption of α-Fe_2O_3. Global fitting extracts 3 component spectra with time constants (τ = 1/k) $\tau_1 = 67 \pm 3$ fs, $\tau_2 = 268 \pm 16$ fs, $\tau_3 = 23.8 \pm 2.1$ ps. Component D is treated as a shelf with an infinite time constant as it does not decay over the 2 nanosecond experimental window. This kinetic model is summarized in the inset to Figure 5A. The IRF-limited first absorption feature (state A) has weak peaks centered at 61.4, 65.5 and 71.5 eV. The second and third component

spectra (states B and C) are almost identical in shape having a main peak at 62.5 eV and shoulders at 60.0 and 65.2 eV, with the main difference being their intensities (Figure 5A). Specifically, state C has 40% lower intensity than state B. The fourth component spectrum (state D) has a similar shape as both B and C but is further reduced in intensity.

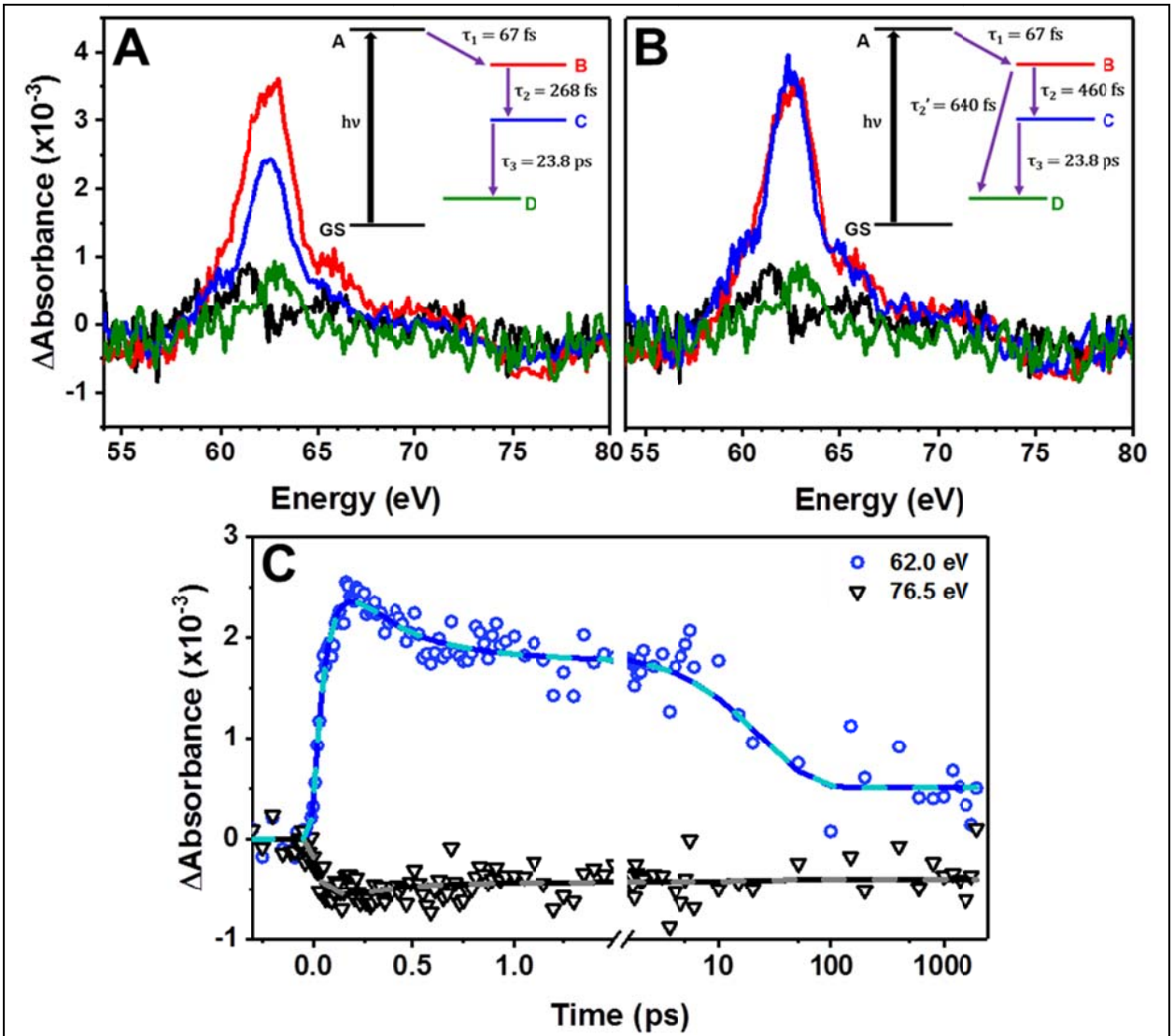

Figure 5: A) Spectral components obtained from the sequential kinetic model. Inset: diagram of the kinetic model with time constants. B) Spectral components obtained from the parallel-pathway model. Inset: kinetic model with time constants. C) Kinetic traces of the data points at 62.0 (blue) and 76.5 (black) eV with the sequential (solid line) and parallel (dashed line) fits.

The similarity between the spectra of states B and C in the sequential model suggest that instead of the system passing through 3 different states, there is another relaxation pathway from state B in the first few ps that results in a reduction in its population. Following this logic, the data was refit to a model with parallel relaxation pathways, as shown in the inset to Figure 5B. State B is assumed to be a vibrationally hot state that either cools to state C or relaxes directly to

D. State C then further relaxes to state D. The extracted spectral components look almost identical to the sequential model fit with changes in scaling of state C. This parallel-model fit yields relaxation rates of τ_2= 460 ± 38 fs for vibrational cooling and τ_2'= 640 ± 19 fs for relaxation to the ground state, with the same rate constants for τ_1 and τ_3 as in the sequential model. The addition of these time constants closely matches τ_2 in the sequential model: $(1/\tau_2 + 1/\tau_2')^{-1}$ = 268 fs.

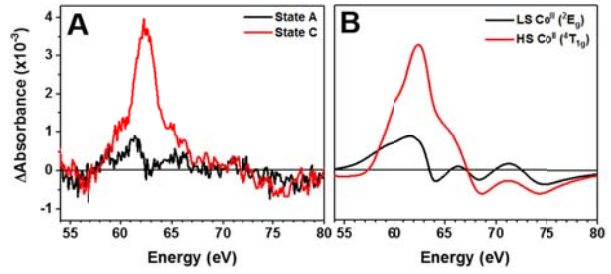

Figure 6: A) Extracted component spectra for states A (black) and C (red). B) LFM simulations of the LS Co^{II}, ^2E_g state (black) and HS Co^{II}, $^4T_{1g}$ state (black).

Both models give an identical fit to the data (Figure 5C). The parallel fit suggests that 40% of the overall population of the vibrationally hot state B relaxes to state D before vibrational cooling, which correlates well with the ~40% reduction in signal intensity between states B and C in the sequential model.

After extracting the spectral components using global analysis, the components were assigned to metal-centered states using LFM simulations and the difference spectrum between the two ground-state isomers. As shown in Figure 6B , the LS Co^{II} (^2E_g) simulation has three weak absorption features centered around 61.9, 66.5 and 71.2 eV, while the HS Co^{II} ($^4T_{1g}$) simulation has a main peak at 62.5 eV with shoulders at 60.0 and 65.6 eV. The simulated LS Co^{II} spectrum matches the component spectrum for state A quite well. Gentili et al. noted that this initial state could alternatively be a Co^{IV} MLCT state. This cannot be entirely ruled out in our results. The LFM method does not accurately calculate the absolute energy of the core-hole state, so tabulated values are used for each element and oxidation state. This treatment could potentially underestimate contributions from exchange stabilization of the core-hole state (see Section S2 for simulated spectra of the Co^{IV} MLCT state). Based on density functional theory and CASSCF/CASPT2 calculations of the electronic structure and coupling between states of similar VT and SCO complexes[12,42], we assign the initial state as the LS Co^{II} (^2E_g) charge transfer state. The later component spectra for states B and C fit well to the GS difference spectrum between the HS Co^{II} and LS Co^{III} tautomers and to LFM simulations of the HS Co^{II} ($^4T_{1g}$) state.

Discussion

The photophysics described above are summarized in Figure 7. 525 nm excitation from the LS Co^{III} ground state forms an LMCT state with LS Co^{II} with an oxidized DQ^{1-} ligand. Intersystem crossing in 67 fs forms vibrationally hot HS Co^{II}. Back-ISC in 640 fs competes with a 460 fs vibrational cooling time that traps molecules in a cold HS Co^{II} state. From there, back-ISC occurs in 23.8 ps. This interplay between intersystem crossing and vibrational cooling has been observed in other transition metal complexes.[43] For example, photoexcitation of $Cr(acac)_3$ leads rapidly to an equilibrium between hot $^4T_2$ and ^2E states via thermally activated intersystem crossing.[44–47] Approximately 20% of the population traps in a cold ^2E state which relaxes in hundreds of ps. An important difference between the $Cr(acac)_3$ and $Co(DQ)_2$ systems should be noted: in $Cr(acac)_3$ the thermally activated back-ISC repopulates an excited state ($^4T_2$), but in $Co(DQ)_2$ the ground state is repopulated.

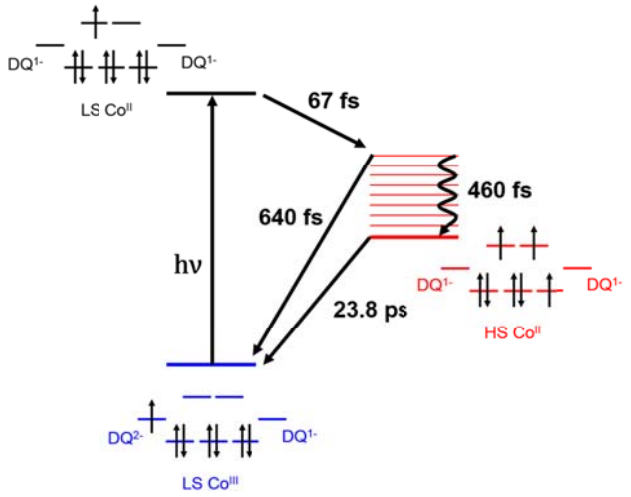

Figure 7: Proposed dynamics of photoinduced valence tautomerization in a $Co(DQ)_2$ thin film

$Co(DQ)_2$ was previously studied by optical transient absorption with ~200 fs time resolution.[15] A time constant of 180 ± 20 fs was reported for the first relaxation step, which we have identified here as LS Co^{II}→HS Co^{II} intersystem crossing. This time constant was likely limited by the IRF or by a slight dependence of the optical signal on the ligand dynamics, and is therefore consistent with the M-edge XANES result. More significantly, the back-ISC lifetime from the cold HS Co^{II} state measured as 410 ps in chloroform solution is significantly slower than the 23.8 ps we measure in a thin film with M-edge XANES. This difference in relaxation times is likely a mixture of solvation and thin-film heating effects. Faster relaxation from the HS Co^{II} state of a similar Co complex has been observed previously in doped polymer films and was attributed to an environment-dependent energy difference between the two tautomers.[48] It is well known that solvation effects play a key role in the valence tautomerization process, and can either change the transition temperature or entirely deactivate the process.[9,49–52] This has been attributed to intermolecular factors such as a change in polarity or lattice softness in crystalline VT compounds, which either changes the barrier or the energy difference between the two tautomers. It is likely that annealing produces one or both effects. The loss of thermal VT in the film suggests a stabilization of the LS Co^{III} tautomer, which lowers the activation barrier for back-ISC. This correlation between energy gap and relaxation time is well known in Fe^{II} systems, and is referred to as the inverse energy gap law.[53] Sample heating also contributes to fast back-ISC in the thin film. As shown in the Supporting Information, optical transient absorption (OTA) data was collected on the same thin film sample used for XUV data collection and gave a 60 ps decay time. The difference in the relaxation times between the OTA and M-edge experiments is likely due to the change from atmospheric convective cooling to cooling by a stream of N_2 in vacuum: the steady-state temperature of the sample is likely higher in the latter, which accelerates the thermally activated back-ISC. The development of in-vacuum thin liquid sheet-jets may soon allow transient XUV spectroscopy to be performed in the solution phase, [54,55] allowing this environment dependence to be tested experimentally.

Conclusion

In summary, femtosecond XUV transient absorption spectroscopy shows that 525 nm excitation of the valence tautomeric complex $Co(DQ)_2$ forms a low-spin Co^{II} LMCT state within the 40 fs instrument response. The complex then undergoes rapid intersystem crossing in 67 fs to a hot high-spin Co^{II} state. Vibrational cooling in 460 fs competes with rapid back-intersystem crossing, with 40% of the excited-state population relaxing to the LS Co^{III} ground state from the hot HS Co^{II} state. The cold HS Co^{II} state relaxes the ground state in 24 ps, with a strong influence from sample temperature and environment. This work showcases the growing importance of ultrafast core-level spectroscopy for transition metal photophysics. The spin

sensitivity of M-edge XANES revealed branching between vibrational and electronic relaxation that was not separable with visible-light probes. The fast time resolution and in-lab convenience of this technique makes it a promising complement to hard X-ray probes of Co complexes.

Acknowledgements

This material is based upon work supported by the National Science Foundation under Grant No. 1555245. The transient XUV instrument, including the nonlinear optical parametric amplifier, was built with funding from the Air Force Office of Scientific Research under AFOSR Award No. FA9550-14-1-0314. We thank Gregory S. Girolami for helpful discussions.

References:

[1] K. Senthil Kumar and M. Ruben, Coord. Chem. Rev. **346**, 176 (2017).

[2] P. Gutlich, Coord. Chem. Rev. **219**–**221**, 839 (2001).

[3] O. Kahn and C.J. Martinez, Science **279**, 44 (1998).

[4] M. Verdaguer, Science **272**, 698 (1996).

[5] O. Sato, T. Iyoda, A. Fujishima, and K. Hashimoto, Science **272**, 704 (1996).

[6] Y. Moritomo, H. Kamioka, T. Shibata, S. Nozawa, T. Sato, and S.I. Adachi, J. Phys. Soc. Japan **82**, 1 (2013).

[7] D.N. Hendrickson and C.G. Pierpont, in *Spin Crossover Transit. Met. Compd. II* (2004), pp. 63–95.

[8] O. Sato, A. Cui, R. Matsuda, J. Tao, and S. Hayami, Acc. Chem. Res. **40**, 361 (2007).

[9] M. Slota, M. Blankenhorn, E. Heintze, M. Vu, R. Hübner, and L. Bogani, Faraday Discuss. **185**, 347 (2015).

[10] S.K. Larsen and C.G. Pierpont, J. Am. Chem. Soc. **110**, 1827 (1988).

[11] H.W. Liang, T. Kroll, D. Nordlund, T.C. Weng, D. Sokaras, C.G. Pierpont, and K.J. Gaffney, Inorg. Chem. **56**, 737 (2017).

[12] D.M. Adams, L. Noodleman, and D.N. Hendrickson, Inorg. Chem. **36**, 3966 (1997).

[13] O. Cador, F. Chabre, A. Dei, C. Sangregorio, J. Van Slageren, and M.G.F. Vaz, Inorg. Chem. **42**, 6432 (2003).

[14] A. Caneschi, A. Cornia, and A. Dei, Inorg. Chem. **37**, 3419 (1998).

[15] P.L. Gentili, L. Bussotti, R. Righini, A. Beni, L. Bogani, and A. Dei, Chem. Phys. **314**, 9 (2005).

[16] N. Azzaroli, A. Lapini, M. Di Donato, A. Dei, and R. Righini, J. Phys. Chem. B **117**, 15492 (2013).

[17] M. Van Veenendaal, Sci. Rep. **7**, 1 (2017).

[18] J. Herrero-Martín, J.L. García-Muñoz, K. Kvashnina, E. Gallo, G. Subías, J.A. Alonso, and

A.J. Barón-González, Phys. Rev. B - Condens. Matter Mater. Phys. **86**, 125106 (2012).

[19] L.C. Wu, T.C. Weng, I.J. Hsu, Y.H. Liu, G.H. Lee, J.F. Lee, and Y. Wang, Inorg. Chem. **52**, 11023 (2013).

[20] W. Zhang, R. Alonso-Mori, U. Bergmann, C. Bressler, M. Chollet, A. Galler, W. Gawelda, R.G. Hadt, R.W. Hartsock, T. Kroll, K.S. Kjær, K. Kubiček, H.T. Lemke, H.W. Liang, D.A. Meyer, M.M. Nielsen, C. Purser, J.S. Robinson, E.I. Solomon, Z. Sun, D. Sokaras, T.B. van Driel, G. Vankó, T.-C. Weng, D. Zhu, and K.J. Gaffney, Nature **509**, 345 (2014).

[21] H.T. Lemke, K.S. Kjær, R. Hartsock, T.B. Van Driel, M. Chollet, J.M. Glownia, S. Song, D. Zhu, E. Pace, S.F. Matar, M.M. Nielsen, M. Benfatto, K.J. Gaffney, E. Collet, and M. Cammarata, Nat. Commun. **8**, 15342 (2017).

[22] P. Wernet, K. Kunnus, I. Josefsson, I. Rajkovic, W. Quevedo, M. Beye, S. Schreck, S. Grübel, M. Scholz, D. Nordlund, W. Zhang, R.W. Hartsock, W.F. Schlotter, J.J. Turner, B. Kennedy, F. Hennies, F.M.F. de Groot, K.J. Gaffney, S. Techert, M. Odelius, and A. Föhlisch, Nature **520**, 78 (2015).

[23] R.M. Jay, J. Norell, S. Eckert, M. Hantschmann, M. Beye, B. Kennedy, W. Quevedo, W.F. Schlotter, G.L. Dakovski, M.P. Minitti, M.C. Hoffmann, A. Mitra, S.P. Moeller, D. Nordlund, W. Zhang, H.W. Liang, K. Kunnus, K. Kubiček, S.A. Techert, M. Lundberg, P. Wernet, K. Gaffney, M. Odelius, and A. Föhlisch, J. Phys. Chem. Lett. **9**, 3538 (2018).

[24] S.E. Canton, K.S. Kjær, G. Vankó, T.B. van Driel, S. Adachi, A. Bordage, C. Bressler, P. Chabera, M. Christensen, A.O. Dohn, A. Galler, W. Gawelda, D. Gosztola, K. Haldrup, T. Harlang, Y. Liu, K.B. Møller, Z. Németh, S. Nozawa, M. Pápai, T. Sato, T. Sato, K. Suarez-Alcantara, T. Togashi, K. Tono, J. Uhlig, D.A. Vithanage, K. Wärnmark, M. Yabashi, J. Zhang, V. Sundström, and M.M. Nielsen, Nat. Commun. **6**, 6359 (2015).

[25] M. Izquierdo, M. Karolak, D. Prabhakaran, A.T. Boothroyd, A.O. Scherz, A. Lichtenstein, and S.L. Molodtsov, Commun. Phys. **2**, 8 (2019).

[26] N.A. Miller, A. Deb, R. Alonso-Mori, J.M. Glownia, L.M. Kiefer, A. Konar, L.B. Michocki, M. Sikorski, D.L. Sofferman, S. Song, M.J. Toda, T.E. Wiley, D. Zhu, P.M. Kozlowski, K.J. Kubarych, J.E. Penner-Hahn, and R.J. Sension, J. Phys. Chem. A **122**, 4963 (2018).

[27] N.A. Miller, A. Deb, R. Alonso-Mori, B.D. Garabato, J.M. Glownia, L.M. Kiefer, J. Koralek, M. Sikorski, K.G. Spears, T.E. Wiley, D. Zhu, P.M. Kozlowski, K.J. Kubarych, J.E. Penner-Hahn, and R.J. Sension, J. Am. Chem. Soc. **139**, 1894 (2017).

[28] K. Zhang, M.F. Lin, E.S. Ryland, M. a. Verkamp, K. Benke, F.M.F. De Groot, G.S. Girolami, and J. Vura-Weis, J. Phys. Chem. Lett. **7**, 3383 (2016).

[29] K. Zhang, G.S. Girolami, and J. Vura-Weis, J. Synchrotron Radiat. **25**, 1600 (2018).

[30] E.S. Ryland, M.-F. Lin, M.A. Verkamp, K. Zhang, K. Benke, M. Carlson, and J. Vura-Weis, J. Am. Chem. Soc. **140**, 4691 (2018).

[31] F. de Groot and A. Kotani, *Core Level Spectroscopy of Solids* (CRC Press, 2008).

[32] K. Zhang, R. Ash, G.S. Girolami, and J. Vura-Weis, ChemRxiv

10.26434/chemrxiv.8259011.v1 (2019).

[33] E.S. Ryland, K. Zhang, and J. Vura-Weis, J. Phys. Chem. A acs. jpca.9b03376 (2019).

[34] C.-M. Jiang, L.R. Baker, J.M. Lucas, J. Vura-Weis, A.P. Alivisatos, and S.R. Leone, J. Phys. Chem. C **118**, 22774 (2014).

[35] J. Vura-Weis, C.M. Jiang, C. Liu, H. Gao, J.M. Lucas, F.M.F. De Groot, P. Yang, a. P. Alivisatos, and S.R. Leone, J. Phys. Chem. Lett. **4**, 3667 (2013).

[36] S. Biswas, J. Husek, S. Londo, E.A. Fugate, and L.R. Baker, Phys. Chem. Chem. Phys. **20**, 24545 (2018).

[37] L.R. Baker, C.-M. Jiang, S.T. Kelly, J.M. Lucas, J. Vura-Weis, M.K. Gilles, A.P. Alivisatos, and S.R. Leone, Nano Lett. **14**, 5883 (2014).

[38] L.M. Carneiro, S.K. Cushing, C. Liu, Y. Su, P. Yang, A.P. Alivisatos, and S.R. Leone, Nat. Mater. **16**, 819 (2017).

[39] J.R. Sutherland, E.L. Christensen, N.D. Powers, S.E. Rhynard, J.C. Painter, and J. Peatross, Opt. Express **12**, 4430 (2004).

[40] R. Santra and A. Gordon, Phys. Rev. Lett. **96**, 073906 (2006).

[41] J. Vura-Weis, C.-M. Jiang, C. Liu, H. Gao, J.M. Lucas, F.M.F. de Groot, P. Yang, A.P. Alivisatos, and S.R. Leone, J. Phys. Chem. Lett. **4**, 3667 (2013).

[42] C. Sousa, C. de Graaf, A. Rudavskyi, R. Broer, J. Tatchen, M. Etinski, and C.M. Marian, Chem. - A Eur. J. **19**, 17541 (2013).

[43] E.A. Juban, A.L. Smeigh, J.E. Monat, and J.K. McCusker, Coord. Chem. Rev. **250**, 1783 (2006).

[44] E.A. Juban and J.K. McCusker, J. Am. Chem. Soc. **127**, 6857 (2005).

[45] E.M.S. Maçôas, S. Mustalahti, P. Myllyperkiö, H. Kunttu, and M. Pettersson, J. Phys. Chem. A **119**, 2727 (2015).

[46] E.M.S. Maçôas, R. Kananavicius, P. Myllyperkiö, M. Pettersson, and H. Kunttu, J. Am. Chem. Soc. **129**, 8934 (2007).

[47] L.S. Forster, Coord. Chem. Rev. **227**, 59 (2002).

[48] D.M. Adams, B. Li, J.D. Simon, and D.N. Hendrickson, Angew. Chemie Int. Ed. **34**, 1481 (1995).

[49] E. Evangelio, C. Rodriguez-Blanco, Y. Coppel, D.N. Hendrickson, J.P. Sutter, J. Campo, and D. Ruiz-Molina, Solid State Sci. **11**, 793 (2009).

[50] E. Evangelio and D. Ruiz-Molina, Comptes Rendus Chim. **11**, 1137 (2008).

[51] C. Boskovic, in *Spin-Crossover Mater. Prop. Appl.*, edited by M. Halcrow, 1st ed. (John Wiley & Sons, Ltd., West Sussex, 2013), pp. 203–224.

[52] O.-S. Jung, D.H. Jo, Y.-A. Lee, B.J. Conklin, and C.G. Pierpont, Inorg. Chem. **36**, 19 (1997).

[53] A. Hauser, Coord. Chem. Rev. **111**, 275 (1991).

[54] J.D. Koralek, J.B. Kim, P. Brůža, C.B. Curry, Z. Chen, H.A. Bechtel, A.A. Cordones, P. Sperling, S. Toleikis, J.F. Kern, S.P. Moeller, S.H. Glenzer, and D.P. DePonte, Nat. Commun. **9**, 1353 (2018).

[55] M. Ekimova, W. Quevedo, M. Faubel, P. Wernet, and E.T.J. Nibbering, Struct. Dyn. **2**, 054301 (2015).

Supporting Information for

Competition Between Intersystem Crossing and Vibrational Cooling in Photoinduced Valence Tautomerism of a Cobalt Dioxolene Complex Revealed with Femtosecond M-edge XANES

Ryan Ash, Kaili Zhang, Josh Vura-Weis

Contents

S1 Optical Transient Absorption

Optical transient absorption (OTA) of $Co(DQ)_2$ was collected by pumping the same film used in the transient XUV experiment along with the same pump fluence at 525nm. In the OTA data, the first 100 fs shows a strong bleach centered at 530 nm followed by a delayed rise of excited-state absorption (ESA) from 600-800 nm. Over time, a reduction in ESA within the first ps similar to the tXUV data is observed. Least-squares fitting a 4-state sequential model used for fitting the tXUV results extracted component spectra shown in Figure S1A with time constants (τ=1/k) of τ_1= 77±1 fs, τ_2= 585±14 fs and τ_3= 60.5±0.5 ps. The data was also fit to a 3-state sequential model which would match a single relaxation pathway from the $^4T_1$ state with time constants of τ_1= 85±1 fs, τ_2= 47.3±0.2 ps. The component spectra from the 3-state model look almost identical to states A, C and D in the 4-state model. The dynamics of the ESA and ground-state bleach (GSB) in the first ps fit much better to the 4-state sequential model at key wavelengths (Figure S1B). Unlike what is seen in M-edge results, the reduction in ESA is relatively small and is accompanied by a change in the shape of the component spectrum. The subtle change in the spectrum at the ps timescale is likely a result of reduction in the $^4T_1$ state population convoluted with other ligand dynamics such as vibrational cooling, which the M-edge spectrum is insensitive to. A difference in timescales between the slower relaxation on the picosecond timescale is likely due to a reduction in cooling in the tXUV experiment, only cooling with a stream of N_2 in vacuum instead of convective cooling in atmosphere.

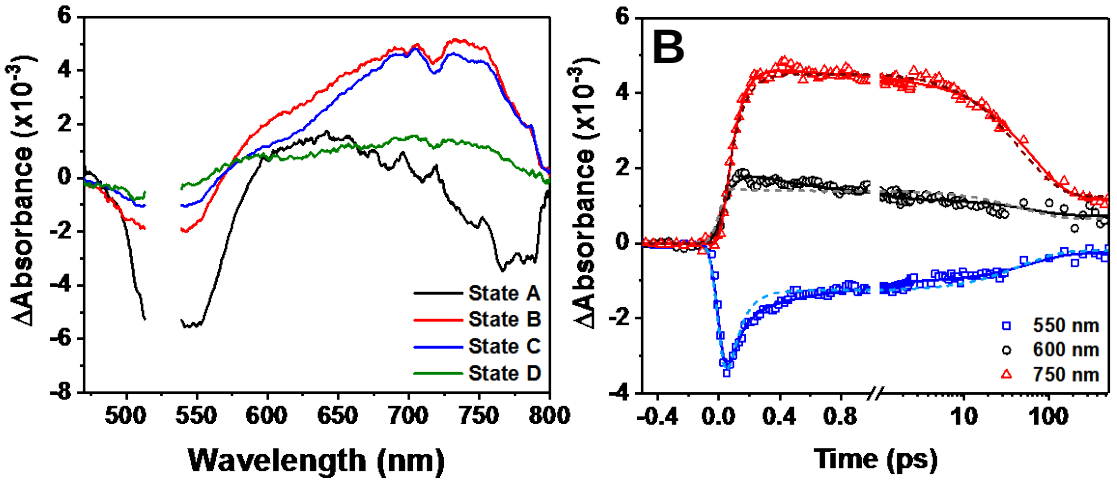

Figure S1: A) Component spectra from a 4-state fit to collected OTA data of $Co(DQ)_2$. B) Traces at key wavelengths with fits to 3-state (dashed) and 4-state (solid) models.

S2 Ligand Field Multiplet Simulation Parameters:

LFM calculations were performed using a customized CTM4XAS program, which has been modified to account for state-dependent core-hole lifetimes.[1–3] Input simulation parameters are shown in Table S1, with the parameters being the ligand field strength (10Dq) and scaling of electron-electron repulsion (F_{dd} and F_{dp}) and exchange (G_{dp}) terms. Post-simulation scaling was performed to account for experimental observations of low-spin spectra being lower in intensity than their high-spin counterparts.

Table S1: Parameters for LFM simulations of the metal-centered states of cobalt

	10Dq (eV)	F_{dd} + F_{pd} scaling	G_{pd} scaling	Intensity Scale
^2E_g (Co^{II} LS)	2.7	80%	100%	70%
$^4T_{1g}$ (Co^{II} HS)	1.5	60%	80%	100%
$^1A_{1g}$ (Co^{III} LS)	2.7	80%	85%	50%
$^2T_{2g}$ (Co^{IV} LS)	2.7	70%	80%	50%

Simulations of the Co^{IV} LS ($^2T_{2g}$) and Co^{II} LS (^2E_g) difference spectra with the estimated horizontal shift in CTM4XAS result in spectra that differ significantly from each other, and would lead to an easy assignment of the first extracted component spectrum as an LMCT state. However, our group has recently observed an MLCT state in $Fe(phen)_3^{2+}$ that matched best with a simulated spectrum that was redshifted by 2-3 eV of the output spectrum[4]. This redshift was attributed to an increase in exchange stabilization of the core-hole state from an increase in the spin of the metal center. If the Co^{IV} LS simulation is shifted by 2.3eV, it gives a reasonable match with the extracted component spectrum of the first state (Figure S2B). While an initial MLCT state in $Co(DQ)_2$ is unlikely, we include this simulation for completeness.

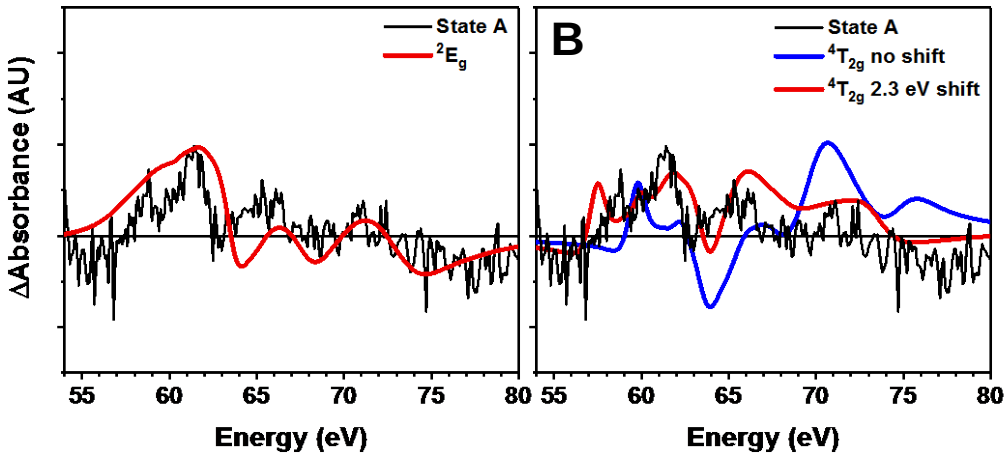

Figure S2: A) Extracted component spectrum for state A (black) along with the LFM simulation for a Co^{II} (^2E_g) LMCT state. B) Extracted component spectrum A (black) along with the unshifted (blue) and shifted (red) simulations for a Co^{IV} ($^2T_{2g}$) MLCT state.

S3 IRF and time-zero determination

Temporal overlap between the pump and probe pulses was determined by monitoring the bleach of the instrument-response limited LMCT transition of α-Fe_2O_3 every 3-4 hours. Traces of the ground state bleach at 57.5 eV were fit to an error function with a negative offset at longer times convoluted with a single exponential decay (Figure S3A). Transient absorption spectroscopy of $Co(DQ)_2$ was collected in 40-minute increments, and the time axis for each such run is corrected by interpolating between the α-Fe_2O_3 references. The full $Co(DQ)_2$ data set is then binned in 10 fs intervals for the first 300 fs and in 20 fs intervals up to 1 ps. Time-zero correction after 1 ps was ignored, where the data was binned in steps of 50 fs or greater. Determination of t_0 for a day of data collection is shown in Figure S3B. Between each $Co(DQ)_2$ run, t_0 did not drift more than 3 fs and drifted in a predictable monotonic fashion.

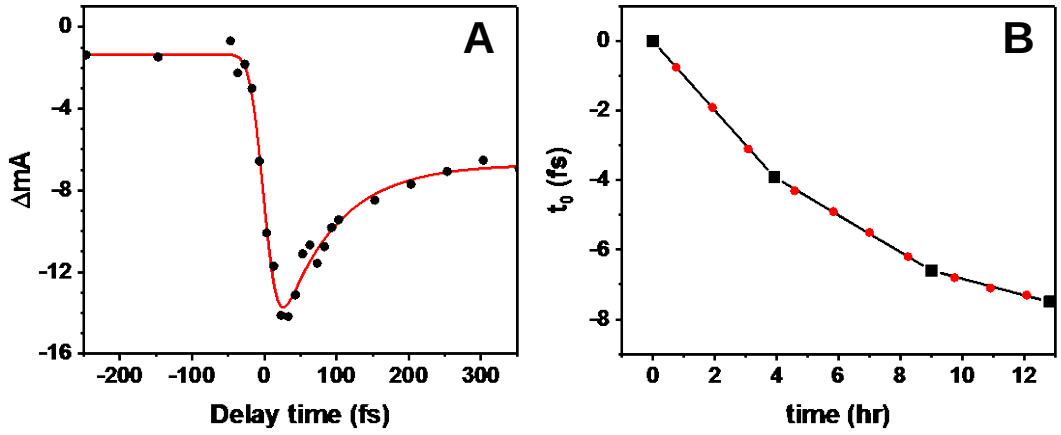

Figure S3: A) Fit (red) of the bleach seen in the transient data (black) of α-Fe_2O_3 pumping at 525 nm. This fit was used to extract t_0 for $Co(DQ)_2$ runs. B) Determination of t_0 for $Co(DQ)_2$ runs (red circles) by linearly interpolating between α-Fe_2O_3 runs throughout the day (black squares).

S4 Comparison between sequential and parallel models

To begin, the two-dimensional data as a function of energy and time is assumed to be a combination of two single-dimensional components. The initial sequential model used to fit the data assuming four different components that flowed linearly from $A \xrightarrow{k1} B \xrightarrow{k2} C \xrightarrow{k3} D$ with corresponding rate constants k1, k2 and k3 and corresponding spectral profiles. Assuming the rate of relaxation from state D is large relative to the observable time window, one is left with the following equations describing the time-dependent population of each species:

$$\frac{d[A]}{dt} = (1 - k_1[A]) \otimes G(t)$$

$$\frac{d[B]}{dt} = (k_1[A] - k_2[B]) \otimes G(t)$$

$$\frac{d[C]}{dt} = (k_2[B] - k_3[C]) \otimes G(t)$$

$$\frac{d[D]}{dt} = (k_3[C]) \otimes G(t)$$

Where [A], [B], [C] and [D] are the populations of states A, B, C and D which is convoluted with the gaussian instrument response G(t). If the model is changed to include another relaxation pathway from state 2 with a separate relaxation time k_2', the rate expressions become:

$$\frac{d[A]}{dt} = (1 - k_1[A]) \otimes G(t)$$

$$\frac{d[B]}{dt} = (k_1[A] - k_2[B] - k_2'[B]) \otimes G(t)$$

$$\frac{d[C]}{dt} = (k_2[B] - k_3[C]) \otimes G(t)$$

$$\frac{d[D]}{dt} = (k_2'[B] + k_3[C]) \otimes G(t)$$

Least squares refinement was carried out using a method based on the variable projection method of Golub and Pereya[5] described below:

With the experimental data Y and standard error W , the spectral components $S = [S_A(\mathrm{E}) \quad S_B(\mathrm{E}) \quad S_C(\mathrm{E}) \quad S_D(\mathrm{E})]$ and time constants $\vec{\alpha} = [\tau_1 \quad \tau_2 \quad \tau_2' \quad \tau_3]$ were determined by minimizing the expression $\|(Y - A(\vec{\alpha})S^T) \circ W\|_F^2$, where $\|\cdot\|_F^2$ denotes Frobenius 2-norm and $\circ$ denotes element-wise product. The matrix $A(\vec{\alpha})$ is a matrix describing the time dependent populations of each state, with each column describing the population of an individual state over time. It can be shown that given a fixed $\vec{\alpha}$, the corresponding optimal is given by

$S^*(\vec{\alpha}) = \left[\vec{s}_A^*(\vec{\alpha}) \quad \vec{s}_B^*(\vec{\alpha}) \quad \cdots \quad \vec{s}_j^*(\vec{\alpha}) \quad \cdots\right]^T$ where $\vec{s}_j^*(\vec{\alpha}) = A^{(j)+}\left(y_j \circ w_j\right)$, $A^{(j)} = \mathrm{diag}\left(w_j\right)A(\vec{\alpha})$, y_j (and w_j) are the j'th column of Y (and W), and $(\cdot)^+$ denotes the Moore-Penrose inverse. Therefore, the problem is reduced to finding the optimal $\vec{\alpha}$ that minimizes $\|(Y - A(\vec{\alpha})S^*(\vec{\alpha})^T) \circ W\|_F^2$. This algorithm was implemented using the SciPy (version 1.2.1) package running on Python 2.7.15.

References

[1] F. de Groot and A. Kotani, *Core Level Spectroscopy of Solids* (CRC Press, 2008).

[2] K. Zhang, G.S. Girolami, and J. Vura-Weis, J. Synchrotron Radiat. **25**, 1600 (2018).

[3] K. Zhang, M.F. Lin, E.S. Ryland, M. a. Verkamp, K. Benke, F.M.F. De Groot, G.S. Girolami, and J. Vura-Weis, J. Phys. Chem. Lett. **7**, 3383 (2016).

[4] K. Zhang, R. Ash, G.S. Girolami, and J. Vura-Weis, ChemRxiv 10.26434/chemrxiv.8259011.v1 (2019).

[5] G.H. Golub and V. Pereyra, SIAM J. Numer. Anal. **10**, 413 (1973).